

Clouds at Arctic Atmospheric Observatories. Part I: Occurrence and Macrophysical Properties

MATTHEW D. SHUPE,* VON P. WALDEN,+ EDWIN ELORANTA,# TANEIL UTTAL,@
JAMES R. CAMPBELL,& SANDRA M. STARKWEATHER,** AND MASATAKA SHIOBARA++

* Cooperative Institute for Research in Environmental Science, and NOAA/Earth System Research
Laboratory, Boulder, Colorado

+ University of Idaho, Moscow, Idaho

University of Wisconsin—Madison, Madison, Wisconsin

@ NOAA/Earth System Research Laboratory, Boulder, Colorado

& Naval Research Laboratory, Monterey, California

** Polar Field Services, Inc., Littleton, Colorado

++ National Institute of Polar Research, Tokyo, Japan

(Manuscript received 6 January 2010, in final form 1 November 2010)

ABSTRACT

Cloud observations over the past decade from six Arctic atmospheric observatories are investigated to derive estimates of cloud occurrence fraction, vertical distribution, persistence in time, diurnal cycle, and boundary statistics. Each observatory has some combination of cloud lidar, radar, ceilometer, and/or interferometer for identifying and characterizing clouds. By optimally combining measurements from these instruments, it is found that annual cloud occurrence fractions are 58%–83% at the Arctic observatories. There is a clear annual cycle wherein clouds are least frequent in the winter and most frequent in the late summer and autumn. Only in Eureka, Nunavut, Canada, is the annual cycle shifted such that the annual minimum is in the spring with the maximum in the winter. Intersite monthly variability is typically within 10%–15% of the all-site average. Interannual variability at specific sites is less than 13% for any given month and, typically, is less than 3% for annual total cloud fractions. Low-level clouds are most persistent at the observatories. The median cloud persistence for all observatories is 3–5 h; however, 5% of cloud systems at far western Arctic sites are observed to occur for longer than 100 consecutive hours. Weak diurnal variability in cloudiness is observed at some sites, with a daily minimum in cloud occurrence near solar noon for those seasons for which the sun is above the horizon for at least part of the day.

1. Introduction

Clouds play an important role in Arctic atmospheric radiation and hydrologic cycles. In addition, complex feedbacks involving clouds have a substantial systemic regional impact on Arctic climate, yet they are not well characterized (Stephens 2005). Clouds may have been influential in recent dramatic Arctic sea ice loss (Kay et al. 2008; Perovich et al. 2008; Schweiger et al. 2008) and their climate influence is sensitive to changes in atmospheric aerosols (e.g., Sassen 2005; Lubin and Vogelmann 2006). Moreover, extended spaceborne observations suggest that Arctic cloudiness is increasing in some seasons while

decreasing in others, resulting in seasonally differential forcing on the Arctic energy balance (Wang and Key 2003). Our understanding of Arctic clouds has been impeded by a paucity of comprehensive observations due to a lack of basic research infrastructure and the harsh Arctic environment, which is characterized by long periods of cold and darkness, blowing snow, and a weak contrast between clouds and the highly reflective surface from satellite perspectives (e.g., Rossow et al. 1993).

When considering the radiative and hydrologic roles of clouds, their relevant properties include cloud presence, vertical and horizontal distributions, temperature, microphysical properties, thickness, and phase composition. Arctic cloud properties have been described in a number of observational studies using aircraft and ground-based remote sensors (e.g., Jayaweera and Ohtake 1973; Herman and Curry 1984; Curry 1986; Hobbs and Rangno 1998;

Corresponding author address: Matthew D. Shupe, R/PSD3, 325
Broadway, Boulder, CO 80305.
E-mail: matthew.shupe@colorado.edu

McFarquhar et al. 2007; Shupe et al. 2001, 2005, 2006; Dong and Mace 2003; Turner 2005). Curry et al. (1996) provide an extensive overview of past Arctic cloud studies and document inconsistencies among the results due to differences in measurement platforms and methods, along with Arctic-specific measurement limitations. It is clear that additional measurements are needed to better understand the general properties and processes of Arctic clouds.

Complementary platforms exist for making detailed Arctic cloud observations, including satellites, ground-based observatories, and manned and unmanned aircraft. Aircraft measurements are most appropriate for case study and process study missions (e.g., Curry 1986; Hobbs and Rangno 1990; Pinto 1998; McFarquhar et al. 2007), for they provide a detailed in situ view of microphysical cloud properties and their covariance with atmospheric state parameters. In the near future, unmanned aerial systems may supplement these capabilities (MacDonald 2005), though they have been impractical to date. Satellite measurements cover a spatial scale that is unmatched by other platforms, with near-global coverage on daily time scales (e.g., Rossow and Schiffer 1991; Stephens et al. 2002). Successful recent deployments of radars (e.g., Stephens et al. 2002) and lidars (e.g., Winker et al. 2003) in space have greatly expanded satellite cloud observational capabilities in the Arctic, although they are ultimately limited by polar-orbital tracks that rarely exceed 81°N. Surface-based remote-sensor observations are unable to match the level of detail from aircraft in situ measurements or the spatial coverage of satellites, yet they are well positioned to capture the diurnal cycle and monitor long-term trends with high temporal and vertical resolutions at fixed locations. We focus here on ground-based remote-sensor cloud observations and describe a statistical characterization of Arctic cloudiness from surface-based measurements at a network of Arctic atmospheric observatories.

The network of Arctic cloud observatories considered here includes past and present sites at Barrow and Atqasuk, Alaska; Eureka, Nunavut, Canada; Ny'Ålesund, Norway; Summit, Greenland; and a yearlong observatory deployed in the permanent ice pack in the western Arctic Ocean. Each observatory employs some combination of cloud radar, lidar, ceilometer, and/or infrared interferometer, each of which provides a unique perspective on clouds. Combining and interpreting the observations from this network is a challenge due to the different sets of instruments, different lengths of observations, and distinct local conditions at each site. Nonetheless, based on the available measurements from these observatories, we present a detailed description of Arctic cloud occurrence, vertical distribution, and macrophysical properties. A related study that focuses on the thermodynamic phase of Arctic clouds is covered in a companion manuscript (Shupe 2011).

Finally, it should be emphasized that, while we present a detailed view of Arctic clouds from surface-based observations, a universal definition of "cloud" is ultimately lacking. Clouds might be defined by a visual requirement such as that employed by surface observers, or based on some minimum density of condensed water or particle size. Similarly, clouds might be identified according to their radiative significance at some wavelength, or by the ability of a sensor to detect a cloud signature. The definition of cloud is entirely dependent upon the perspective and objective. Here, we simply define clouds as those that can be distinguished from clear air by stationary, zenith-pointing remote-sensor measurements using the methods and thresholds that are described, which are closely related to instrument specifications. In most cases these techniques have been designed to provide the highest possible cloud occurrence fraction while limiting false positive identifications. The zenith-viewing perspective of the ground-based remote sensors should be kept in mind for all results presented here. Cloud fraction, from this perspective, is defined as the fraction of time clouds are observed by the zenith-pointing instruments.

2. Cloud observations

a. Observatories

A number of permanent and temporary atmospheric observatories, each with unique cloud-observing instrument suites, have been established across the Arctic over the past decade (Table 1 and Fig. 1). The spatial distribution of these sites provides an opportunity to observe clouds in a wide variety of Arctic meteorological and topographic conditions. However, without a dense network of such observatories, it is difficult to assess how representative these locations are of the pan-Arctic or even regional cloudiness.

The observatory in Barrow is located on the northern coast of Alaska with limited local topography, leading to cloudiness that can be either marine or continental in nature depending upon the large-scale flow. Its sister observatory at Atqasuk is ~100 km inland yet still 400 km north of the Brooks Mountain Range, resulting in cloudiness that is more continental in nature. While Barrow has a much more extensive instrument suite, these two sites have been in operation for more than 10 yr and provide the longest record of clouds included in this study. Located on a fjord, the Eureka observatory might be considered coastal; however, on a regional scale this site is embedded within the Canadian archipelago, which includes a complex system of islands and waterways with highly variant topography and surface types. The instruments used here have been in operation at Eureka

TABLE 1. Arctic atmospheric observatories. For the fourth column, the date range is for the suite of cloud-observing instruments considered here, which may not be identical to the operation of the site as a whole.

Site name	Site location	Coordinates	Dates of operation	Dates used in study	Instruments
Atqasuk	North Slope of AK	70°28'N, 157°24'W	October 1999– present	October 1999– September 2009	Ceilometer, MWR
Barrow*	North Slope of AK	71°19'N, 156°37'W	March 1998– present	March 1998– September 2009	MMCR, MPL, ceilometer, AERI, MWR
Eureka*	Ellesmere Island, NU, Canada	80°00'N, 85°57'W	August 2005– present	August 2005– September 2009	MMCR, HSRL, AERI, MWR
Ny'Alesund	Svalbard, Norway, in the North Atlantic	78°55'N, 11°56'E	March 2002– present	March 2002– May 2009	MPL
SHEBA*	Beaufort and Chukchi Seas in the western Arctic Ocean	75°–80°N, 143°–167°W	October 1997– October 1998	October 1997– October 1998	MMCR, DABUL, ceilometer, AERI, MWR
Summit	Greenland	72°34'N, 38°29'W	June 2001– April 2002	June 2001– April 2002	Ceilometer

* Supersite, considered as such because it includes a suite of instruments that can observe the vertical distribution of cloudiness.

since late summer of 2005. Ny'Alesund is on the western coast of Svalbard, a Norwegian archipelago located north of Scandinavia in the Greenland and Barents Seas. Its local climate is thus influenced by marine and Arctic air masses, the complex terrain of Svalbard, and the Greenland landmass, which lies ~700 km to the west. Limited cloud observations have been made there since 2002. At 3.2-km elevation, Summit station is perched atop the Greenland ice sheet in a location like none other in the Northern Hemisphere. Only about 1 yr of cloud observations are available from this site, providing only a brief snapshot of clouds over the Greenland ice sheet. Finally, we include a ship-based observatory that drifted with the permanent ice pack in the western Arctic Ocean as part of the yearlong Surface Heat Budget of the Arctic (SHEBA; Uttal et al. 2002) project, providing a purely Arctic Ocean sea ice environment for observing clouds. Like Summit, the SHEBA observations were limited to only 1 yr. While both the Summit and SHEBA observations cannot be considered representative of clouds at these sites, they are the only observations available for these locations and are thus a valuable component of this study. All results pertaining to these sites should be considered within the context of their limited length of observations.

Three of the stations (Barrow, Eureka, and SHEBA) are referred to, henceforth, as supersites because they contain a sufficient suite of instruments to observe the vertical distribution of cloudiness. All references to height are "above ground level," which for all stations other than Summit is within a few tens of meters of mean sea level.

b. Instruments and detection algorithms

Each atmospheric observatory includes one or more ground-based cloud-observing instruments. While no single instrument can provide a complete view of cloudiness,

the combination of sensors at certain sites provides a reasonably comprehensive perspective. Each instrument used in this study has a unique set of specifications that define its ability to observe clouds. Therefore, each system requires a unique method to distinguish cloudy from clear-sky observations. This study, when possible, uses documented and referenced cloud identification algorithms and datasets that are broadly available and recognized by the research community. Key instrument specifications and methods are briefly outlined here, with special attention given to those methods that are not well documented elsewhere. All instruments and their pertinent measurements utilized in this study are summarized in Table 2.

1) RADAR

Radar observations are used here for identifying cloud presence, boundaries, and total thickness. All three of the



FIG. 1. Map showing Arctic observatories.

TABLE 2. Instruments, measurements, and pertinent specifications for all datasets used in this study. Here, Δz and Δt are the vertical and temporal resolutions.

Instrument	Measurements	Sites	Pertinent specifications	Derived parameters
MMCR	Reflectivity, signal-to-noise ratio	Barrow, Eureka, SHEBA	$\Delta z = 45\text{--}90$ m, $\Delta t = 4\text{--}10$ s	Presence, boundaries
HSRL	Backscatter, depolarization ratio	Eureka	$\Delta z = 30$ m, $\Delta t = 30$ s	Presence, boundaries
DABUL	Backscatter, depolarization ratio	SHEBA	$\Delta z = 30$ m, $\Delta t = 5$ s	Presence, boundaries
MPL	Backscatter, depolarization ratio (Barrow only)	Barrow, Ny'Alesund	$\Delta z = >5$ m, $\Delta t = >2$ s	Presence, boundaries
Ceilometer	Backscatter	Atqasuk, Barrow, SHEBA, Summit	$\Delta z = 15$ m, $\Delta t = 15$ s	Presence, cloud base
AERI	IR radiance/ T_B	Barrow, Eureka, SHEBA	$\Delta t = 30$ s	Presence
MWR	T_B	Barrow, Eureka, SHEBA	$\Delta t = 30$ s	Presence (support)

35-GHz millimeter cloud radars (MMCR; Moran et al. 1998) used here are effectively duplicates of each other with nearly identical operational characteristics. Examination of radar measurements to identify clouds and their vertical locations is done within the context of the Active Remote Sensing of Cloud Layers (ARSCL) algorithm (Clothiaux et al. 2000). In short, cloud returns are identified if the radar signal is distinguishable from the receiver noise, then significant signals from multiple operational modes are optimally combined into a comprehensive cloud product for all times and heights. Only radar reflectivities higher than -60 dBZ are considered when identifying clouds. Because of sensitivity limitations, radars sometimes fail to detect clouds with low concentrations of small particles (some thin liquid layers and high ice clouds) because of their small radar backscatter cross section. Thus, radar estimates of cloudiness may be biased low but are unlikely to be biased high.

While MMCR data from all sites were processed using the ARSCL algorithm, an additional filter was used to minimize the impacts of spurious, yet frequent, low-reflectivity returns near the surface that are likely due to near-field noise related to internal radar switches (K. Moran 2010, personal communication). To address this issue, a requirement was added based on comparisons with collocated remote sensors that some range gate within the lowest six (~ 300 m) must contain a reflectivity higher than -40 dBZ for any of those range gates to be considered cloudy.

2) LIDAR

Each observatory in this study operates at least one laser-based system for observing clouds; these range from ceilometers to fully calibrated lidars. The basic principle for cloud-layer detection using laser-ranging measurements is to relate signal magnitude and its change with height to the background atmospheric, or molecular,

scattering structure and noise inherent to a given profile. Thresholds are then optimized to distinguish cloud particle scattering from that of clear skies and aerosols. Lidar wavelengths are readily attenuated by clouds, with full occultation at an optical depth of 3–5 (e.g., Sassen and Cho 1992), preventing higher-altitude observations in optically thick cloud systems. On the other hand, the sensitivity of lidar wavelengths to small particles is quite good, allowing lidar to detect thin, tenuous clouds composed of small particles and atmospheric aerosol particles. Unfortunately, at lidar wavelengths some clouds are optically thinner than some aerosol layers. Invariably, due to the cloud-detection thresholds and filters that are employed, some fraction of thin cloud layers may be missed while particularly thick aerosol layers may be falsely identified as a cloud. In general, lidar systems are well suited to observe the presence of clouds and the cloud-base height.

At Barrow, the micropulse lidar (MPL; Campbell et al. 2002) signal was examined for cloud returns within the same ARSCL framework described above according to the method detailed by Clothiaux et al. (1998). That routine identifies clouds relative to an estimated clear-sky profile derived from the closest-in-time clear-sky measurements. Therefore, the algorithm is independent of calibration and instrument drift in time. MPL observations from Ny'Alesund are processed with the standard micropulse lidar network (MPLNET; information online at mplnet.gsfc.nasa.gov) algorithm, which combines a basic threshold–signal-slopetechnique, for data with relatively high signal-to-noise ratios (Welton and Campbell 2002), with a more complex threshold-based methodology applied to low signal-to-noise data based on the uncertainties of the MPLNET level 1 data product (Campbell et al. 2002, 2008). This method is unable to quantitatively resolve signals below ~ 300 m. For cases when the signal was deemed to be attenuated below this height,

TABLE 3. HSRL cloud identification thresholds.

Parameter	Threshold
Molecular count signal-to-noise ratio	>5
Backscatter signal-to-noise ratio	>10
Total backscatter	$>1 \times 10^{-7} \text{ m}^{-1} \text{ sr}^{-1}$
Layer optical depth	>0.03
Backscatter for neighboring time-height pixels	At least three of nine, $>5 \times 10^{-7} \text{ m}^{-1} \text{ sr}^{-1}$; at least one of nine, $>1 \times 10^{-6} \text{ m}^{-1} \text{ sr}^{-1}$

a hydrometeor layer was assumed to be present and to have caused the signal blockage.

Lidar measurements in Eureka were made with a high-spectral-resolution lidar (HSRL; Eloranta 2005). Observations at 30-m and 30-s resolutions were used to identify cloudy pixels using the suite of filters outlined in Table 3. For cloud detection, the first pixel within a vertical column with backscatter greater than $10^{-7} \text{ m}^{-1} \text{ sr}^{-1}$ is used to adjust the HSRL-accumulated optical depth profile to 0. During SHEBA, the depolarization and backscatter unattended lidar (DABUL; Intrieri et al. 2002) collected observations for much of the yearlong campaign. The cloud-layer dataset described by Intrieri et al. (2002) was used, wherein clouds were distinguished manually from noise based on a visual inspection of the imagery. In

addition, Vaisala ceilometers were in operation at four observatories (Atqasuk, Barrow, SHEBA, and Summit). For each of these instruments, the standard cloud-base detection algorithm provided by Väisälä was employed to identify both the presence of cloudiness and the lowest cloud-base height.

3) AERI

Atmospheric Emitted Radiance Interferometer (AERI; Knuteson et al. 2004) measurements relate to the direct effects of clouds on IR radiances, and all systems used here are nearly identical. Thus, AERI-derived cloud fractions represent those clouds that affect the surface downwelling IR radiation. AERI measurements provide a column perspective only and do not yield zenith-profile information, as with the active sensors. AERI measurements are, therefore, only used here to identify cloud presence. AERI cloud identification is based on a precipitable water vapor (PWV) dependent brightness temperature threshold technique developed for the three supersites. The PWV used to support AERI observations is derived from 23- and 31-GHz sky brightness temperature measurements made by two- or five-channel microwave radiometers (MWRs; Liljegren 1994).

To derive this threshold relationship, clear-sky time periods were identified using a combination of radar and lidar observations, with a requirement of clear sky for at

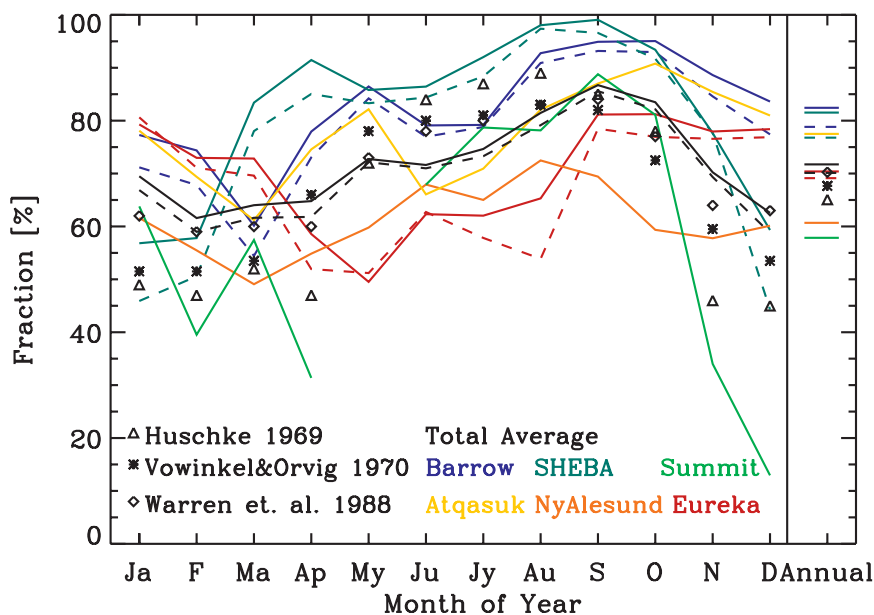


FIG. 2. Annual cycle of monthly mean cloud occurrence fraction at six Arctic atmospheric observatories. For those sites with multiple cloud sensors, a cloud fraction for only lidar systems is provided as the dashed curve. The average cloud fraction for all sites, equally weighting each site, is given as the black curve. Annual average cloud fractions for each dataset are provided at the right. For comparison, past Arctic cloud fraction climatologies are also provided from Huschke (1969), Vowinkel and Orvig (1970), and Warren et al. (1988).

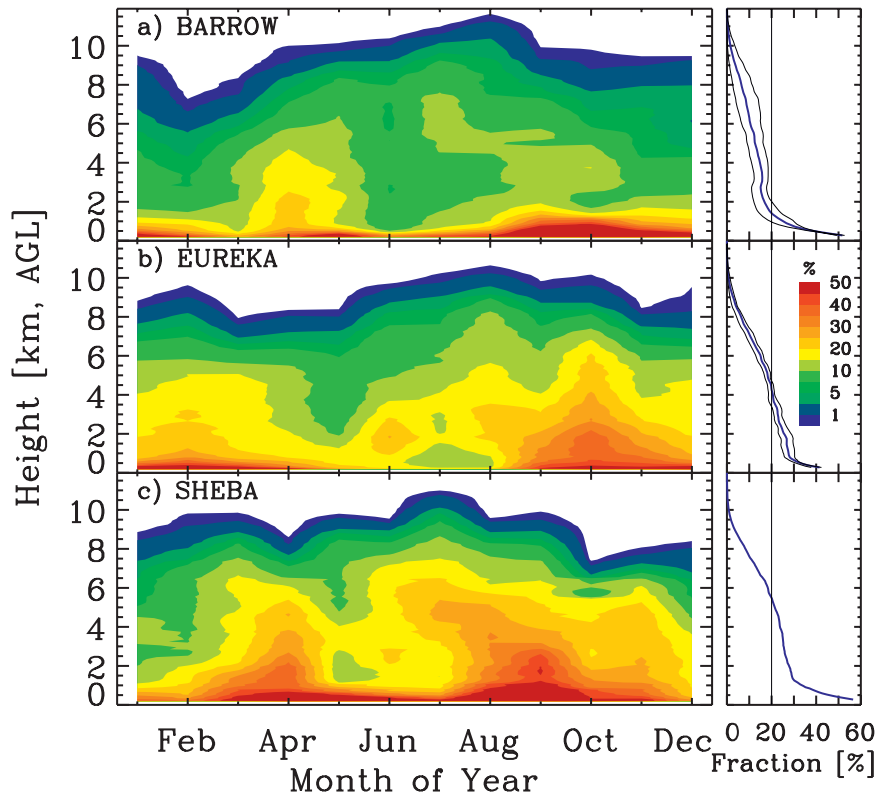


FIG. 3. Cloud vertical distribution: (a) Barrow, (b) Eureka, and (c) SHEBA. The contour plots show the average cloud occurrence fraction as a function of month and height. Shown at the right are the annual average profiles for each station (blue line) surrounded by the range of values from individual years as a function of height (black lines). A vertical line is provided at 20% for comparison purposes.

least ± 15 min from the time of interest. For this clear-sky dataset, AERI brightness temperatures at 900 cm^{-1} and the microwave radiometer-derived PWV were fit using a quadratic polynomial. The resulting relationship is $T_{B900} = 138.18 + 50.61\text{PWV} - 10.02\text{PWV}^2 + 10$, where PWV is in centimeters, the threshold brightness temperature is in degrees kelvin, and the 10 degrees added to the relationship adjust the threshold to capture clear-sky brightness temperatures. For the clear-sky dataset from all three sites, only 2.6% of the observations had brightness temperatures warmer than this threshold relationship. While there is the possibility that some of these data points may result in false positive cloud identifications, it is also possible that some of the “clear sky” observations were contaminated by cloudy-sky cases that were not detected by the active remote sensors.

c. Best-estimate parameters

Cloud observations from each instrument are optimally combined to give 6-hourly “best estimate” parameters. For cloud fraction, the highest value is used from the set of instruments that operated for at least 80% of a 6-h time

period. If no instrument passed the 80% criterion, the highest cloud fraction from those instruments with any amount of operational time is used. For the lowest cloud-base height, if the radar cloud base is below 5 km, the best estimate is considered the lowest cloud base from the laser-based systems because the radar base might be contaminated by precipitation. If the radar base is above 5 km, then the lowest of the radar and lidar bases is used. For high cloud tops, the maximum of the radar or lidar high cloud tops is used because either of these could see the highest top depending on the specific conditions. Finally, for total cloud thickness, the maximum of the radar or lidar thicknesses is used, except that the radar thickness is diminished by the difference between the lowest radar cloud base and the best-estimated cloud base if it is higher to avoid the inclusion of precipitation.

3. Results

a. Cloud occurrence

Cloud occurrence fraction, or simply cloud fraction, is a fundamental parameter with important bearing on the

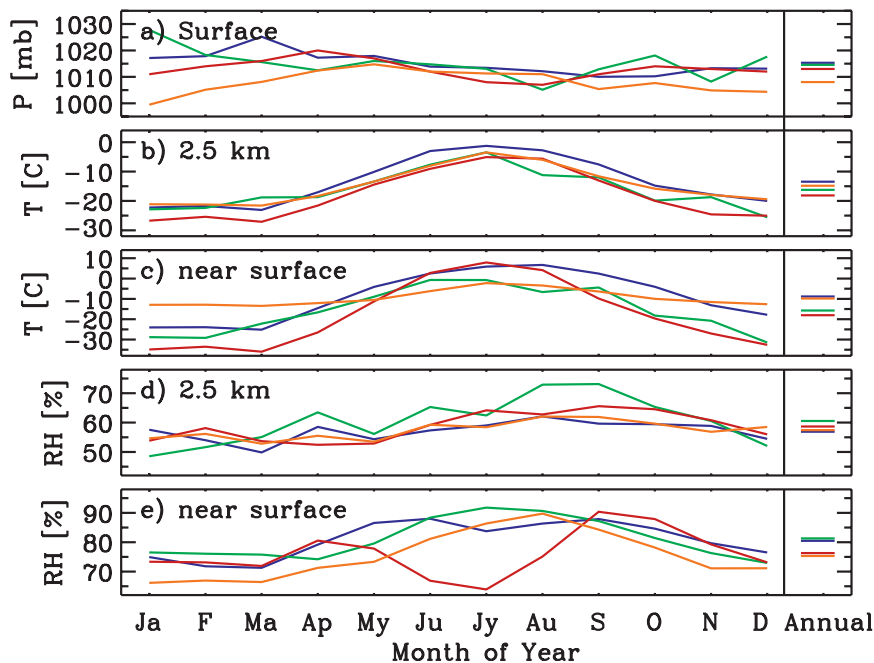


FIG. 4. Annual cycles of monthly mean (a) surface pressure, (b) temperature at 2.5 km, (c) temperature near the surface, (d) relative humidity at 2.5 km, and (e) relative humidity near the surface for Barrow (blue), SHEBA (green), Ny'Alesund (orange), and Eureka (red). Results are derived from 10 yr of surface and radiosonde measurements at the three permanent Arctic observatories, but only 1 yr of observations from SHEBA.

many roles that clouds play in the climate system. Annual cycles of the best-estimated average monthly cloud fraction for each Arctic observatory are given as solid lines in Fig. 2 along with the total annual cloud fractions. These annual cycles are based on the available data for each location, which can range from a decade at Barrow down to only about 1 yr for the SHEBA and Summit observations. For these later two sites, the interannual representativeness of the available observations is currently unknown. An all-site average of monthly cloud fraction (equally weighting each site) yields the solid black curve in Fig. 2. The total annual cloud fraction at the Arctic observatories ranges from 58% to 83%. For comparison, three climatologies of Arctic cloud fraction derived from surface-based observations are also provided in Fig. 2 (Huschke 1969; Vowinkel and Orvig 1970; Warren et al. 1988). The all-site average cloud fraction curve is similar to the Arctic cloud climatology described by Warren et al. (1988), with monthly differences of no more than 8%, seasonal variations that are nearly identical, and total annual cloud fractions within a few percent. Additionally, the combination of radar and lidar at the supersites offers the added capability to characterize the vertical distribution of cloud fraction, which is shown in Fig. 3.

At most observatories, there exists a late summer or fall cloud occurrence maximum, whereas the annual

minimum typically varies from December through March depending on the site. This cycle is linked to the annual variations in the broader meteorology at these sites, as characterized by the annual cycles of monthly averaged atmospheric pressure, temperature, and moisture given in Fig. 4, and may also be related to strong annual variations in surface state and sunlight. At all supersites, and in nearly all months, the total cloud fraction increases with decreasing altitude. Annual average vertical distributions (right panels in Fig. 3) show a steady increase with decreasing altitude, with a relatively sharp increase below about 1 km. The highest clouds in any season tend to track the annual variation in tropopause height. Summer maximum cloud heights extend up to 10–11 km at all sites.

Sites in the far western Arctic (Atkasuk, Barrow, and SHEBA) have similar annual cycles and total annual fractions near 80%. These locations all have spring (April–May) local maxima with a subsequent drop in cloud occurrence prior to an increase toward the late summer annual maximum. Cloud occurrence minima occur in winter and early spring at ~60%, whereas the seasonal variability over the annual cycle (the annual amplitude) is 30%–40%. The year of observations at SHEBA showed more frequent occurrences of midlevel clouds than at Barrow, leading to higher overall cloud fractions during the spring and summer months. On the other hand, the

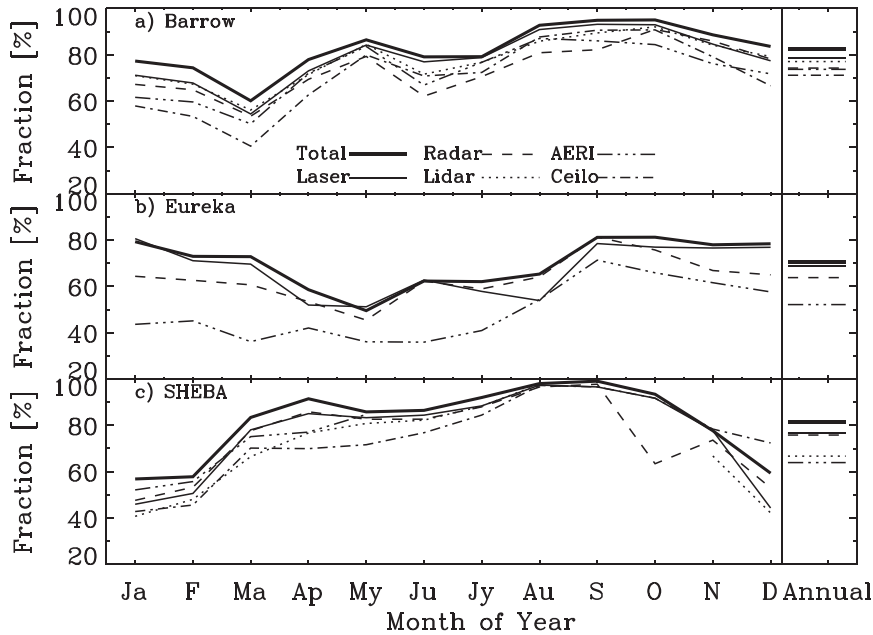


FIG. 5. Annual cycles of monthly mean cloud occurrence fraction at the (a) Barrow, (b) Eureka, and (c) SHEBA Arctic observatories distinguished by instrument. Annual means are given at the right. In some months the cloud fraction for a given instrument is positively or negatively biased because of undersampling by that instrument. In the right portion of (c), the ceilometer annual cloud fraction is hidden behind the line for the laser cloud fraction.

winter at SHEBA yielded fewer low-level clouds than typically occur at Barrow. These annual trends at the western Arctic sites can be explained by the typical annual variations of meteorological parameters at these sites, with relatively high surface pressure, cold temperatures, and low moisture in the winter, and the opposite during summer. Even finer details of the cloud occurrence are reflected in the meteorology, such as the correspondence of the highest monthly averaged surface pressure with the lowest monthly averaged cloud fraction (Fig. 4a), which occurred at a different month during SHEBA relative to Barrow.

As one moves toward the east, the amplitude of the annual cycle of cloudiness in Eureka is similar to the far western Arctic observatories, yet the cycle itself is shifted temporally. Whereas the annual minimum monthly cloud fraction at other sites occurs in winter (December–March), it occurs in May at Eureka. Moreover, the total cloud fraction remains high and relatively constant from September through March (at $78 \pm 5\%$). This annual cycle is in contrast to that for the “Canadian Arctic” given by Huschke (1969), which follows a cycle similar to the “central Arctic” Huschke data in Fig. 2, albeit with slightly lower values in all seasons.

The unique annual cloudiness trend at Eureka is a result of a marked decline in low-level cloudiness at that site during the summer. Overall, low-level clouds occur

about 40% of the time at this site, but summer fractions decrease to less than 20%, contributing to the lower summer cloud fraction relative to the other sites. In the winter, it is the midlevel clouds that lead to the relatively high cloud fraction in Eureka in comparison with the other stations. Finally, the May cloudiness minimum at Eureka is seen to extend throughout the vertical column

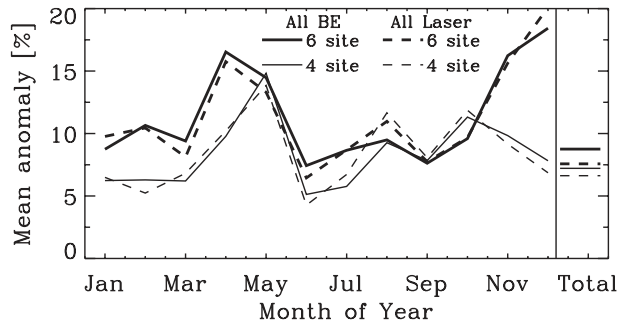


FIG. 6. Annual cycles of the intersite variability of cloud occurrence fraction. Lines show monthly mean absolute cloud fraction anomalies based on the total best-estimate cloud fraction (solid lines) and the laser-only cloud fraction (dashed lines) for all six observatories (thick lines) and for only the four observatories with multiple years of observations (thin lines). Annual means are given at the right. Anomaly is defined here as the absolute difference between a total monthly cloud fraction at a given site relative to the all-site mean.

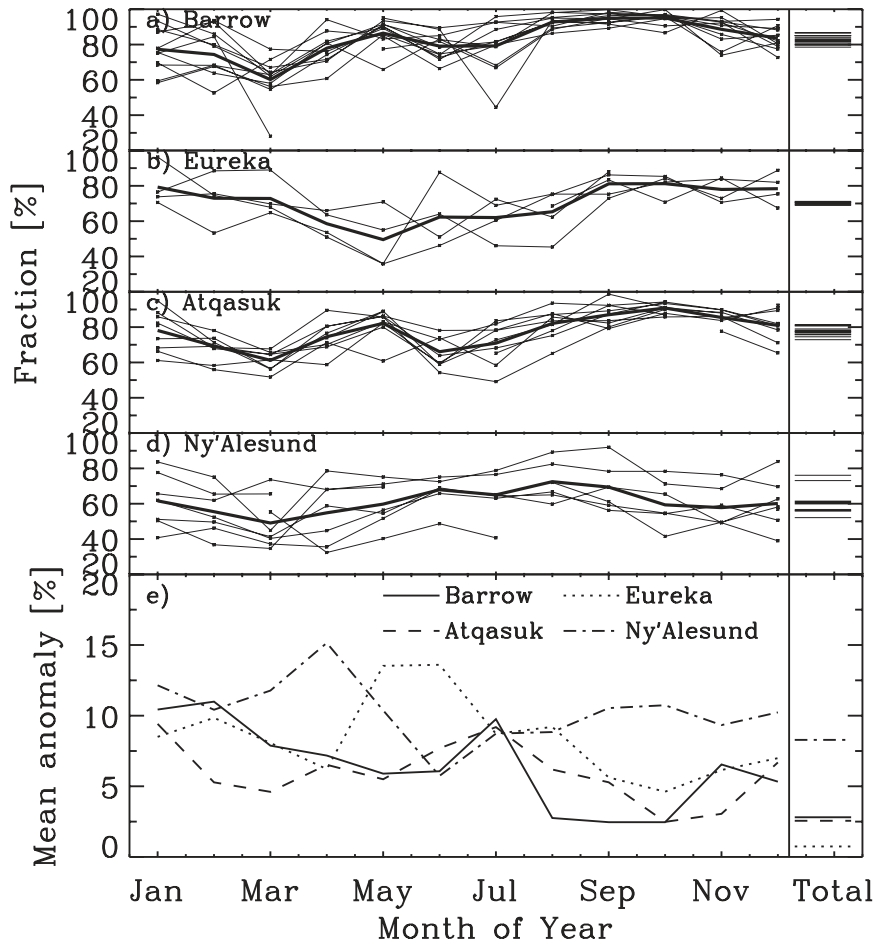


FIG. 7. (a)–(d) Annual cycles of the interannual variability of cloud occurrence fraction for the four locations indicated. The site average annual cycle of the monthly mean cloud occurrence fraction is given (thick line), as well as individual yearly monthly means (dots connected by thin lines). For each time period (month or year), there must be at least 75% data available for a data point to be included. (e) The mean interannual cloud fraction anomalies for the four stations. In (a)–(e), annual means are given at the right. Anomaly is defined here as the absolute difference between any given monthly mean (e.g., January 2005) relative to the total monthly mean (all Januarys).

(Fig. 3b), while a similar midlevel cloud occurrence minimum is observed in June at Barrow and in May during SHEBA. From a meteorological perspective (Fig. 4), the highest monthly surface pressure and the lowest monthly midlevel relative humidity at Eureka are in the spring, coinciding with the cloud fraction minimum. While these parameters are not extremely different from the values observed at the other sites, the near-surface relative humidity at Eureka does show a significant drop in the summer, contributing to the minimal low-level cloud fraction during that time.

The two easternmost sites also exhibit unique cycles of cloudiness. At Ny'Alesund, the annual cycle is similar to many of the other sites, but the amplitude is only 24%, with an annual cloud fraction of 61%. This cycle is similar

to the “Norwegian Seas” clouds documented by Vowinkel and Orvig (1970) for the region south of Svalbard. However, the observed cycle at Ny'Alesund is offset by 1 month, has larger annual amplitude, and has a lower total cloud fraction. The gradual increase in summer cloudiness at Ny'Alesund is coincident with an increase in relative humidity at the site in spite of the summertime weakening of the Icelandic low (Fig. 4). Relatively small annual changes in the basic meteorological parameters at Ny'Alesund likely contribute to the relatively small annual amplitude of the monthly cloud fractions.

The observations from Summit, on the other hand, show a large cloud fraction annual cycle amplitude. Summer cloud amounts are comparable with the other sites but winter amounts are significantly lower. With less than 1 yr

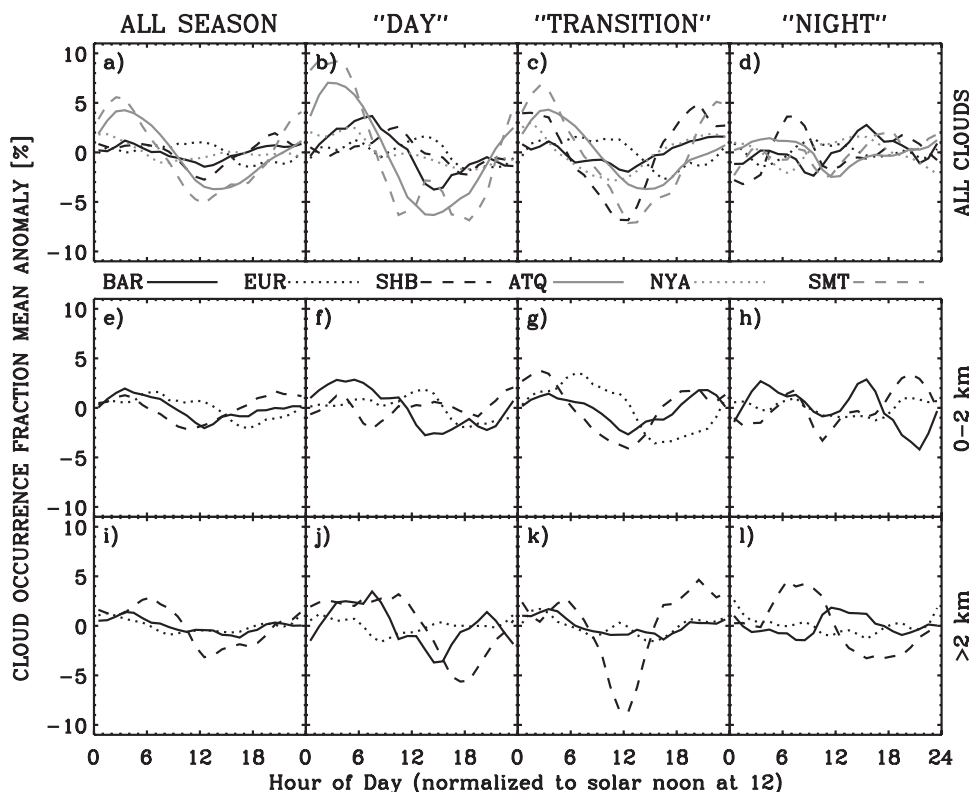


FIG. 8. Diurnal cycle of cloudiness. All panels show the diurnal cloud occurrence fraction anomaly (hourly mean minus daily mean). Columns are labeled at the top and are defined as (a),(e),(i) all clouds; (b),(f),(j) day, which requires the sun to be above the horizon for the full day; (c),(g),(k) transition, which requires the sun to be both above and below the horizon within a given day; and (d),(h),(l) night, which requires the sun to be below the horizon for the full day. Rows are labeled to the right. The top row pertains to all clouds at all heights for all observatories. The bottom two rows are for clouds below and above 2 km at the three supersites only. Observations at each site have been adjusted such that 12 on the plot axis is approximately the lowest daily SZA for each site. Approximate solar noontimes (in UTC) at each site are Atqasuk and Barrow, 2230; Eureka, 1745; Ny'Alesund, 1115; Summit, 1445; and SHEBA, 2245–2315.

of Summit observations, it is not possible to determine how representative these measurements may be of the climatological cloudiness at the site. Putnins (1970) indicated winter cloud fractions at a camp about 100 km southwest of Summit (though still on the central Greenland ice sheet) to be in the 40%–50% range.

b. Instrumental implications for cloud occurrence fraction

Each observatory has a unique suite of instruments that defines its ability to observe clouds. A comparison of monthly average cloud fractions for each instrument at the three supersites is shown in Fig. 5. In broad terms, all instruments tend to capture the seasonal cycle of cloudiness with typical agreement to within $\sim 20\%$ in most months. For Barrow and SHEBA, no instrument consistently observes more cloudiness than another, although the combined “laser based” cloud fraction (which

combines lidar and ceilometer) is typically higher than others. During October at SHEBA, the radar had a smaller temporal sample size than the other instruments, leading to marked differences in cloud fraction during that month. At Eureka, the lidar cloud fractions are higher than the radar cloud fractions by 10%–15% from November through March, whereas the radar cloud fractions are slightly higher in the late summer, due in part to recurring lidar component failures, leading to undersampling during those months. Lidar sampling issues during May and June at Eureka also lead to a lidar cloud fraction that is slightly larger than the best-estimated total cloud fraction. The AERI estimate is generally much lower than those from the other instruments at Eureka. These results indicate that the AERI cloud-detection method, which was determined using data from all three supersites, may be insufficient for detecting clouds at Eureka and/or that many clouds in Eureka have an undetectable

radiative signature in the infrared. Consequently, no significant change is realized if the polynomial clear-sky threshold fit is constructed using only AERI observations from Eureka. Clearly, further work on the subject is warranted.

The intersite comparison of cloud fraction given in Fig. 2 is complicated by the disparity of instruments at each observatory and the unique perspective that each instrument has on cloudiness (Fig. 5). The simplest way to compare cloudiness among the sites is to consider only the laser-based instruments since they all operate at similar wavelengths and detect clouds based on the same principle (vertical changes in backscattered visible or near-IR light). However, there are still important caveats to consider when comparing sites in this way. For the two sites where comparisons between the collocated lidar and ceilometer can be made (SHEBA and Barrow), the monthly and annual cloud occurrence fractions are typically within 10% or better, but sometimes as high as 15% (Fig. 5). This suggests that, on average, cloud fraction differences among the laser-based systems from different sites are on the order of 10%. In addition, the instrument comparisons at the supersites (Fig. 5) suggest that lidars may underreport cloudiness by as much as 15%, though typically less than 10%, in any month relative to the best estimate. Comparisons of laser-based cloud fraction from the supersites are included in Fig. 2 as dashed curves. In each case the monthly cloud fractions are different from the best estimate by less than 10%, yet the general annual trends are the same. The mean, all-site cloud fraction (black dashed curve in Fig. 2) decreases by $\sim 2\%$.

c. Intersite and interannual variability of cloud occurrence

In terms of spatial variations, the intersite variability from the all-site mean is similar for both the best-estimate and laser-derived cloud fractions (comparison of thick solid and dashed lines in Fig. 6). From either perspective, the mean absolute cloud fraction anomaly, which is a measure of site-to-site variability, is about 10% in all months except for April, May, November, and December, when the mean anomalies reach more than 15%. Some of this variability is due to the single-year observations from Summit and SHEBA, which may not fully represent those sites. By not including these sites (thin lines in Fig. 6), the intersite variability is $\sim 10\%$ in all months except for May, highlighting the distinct minimum at Eureka in that month. These data, therefore, indicate that in any given month the cloud occurrence fractions at these Arctic sites can vary by about 10% from the all-site average cloud fraction. This is somewhat less than the spatial variability of the cloud fraction derived from satellite observations by Wang and Key (2005).

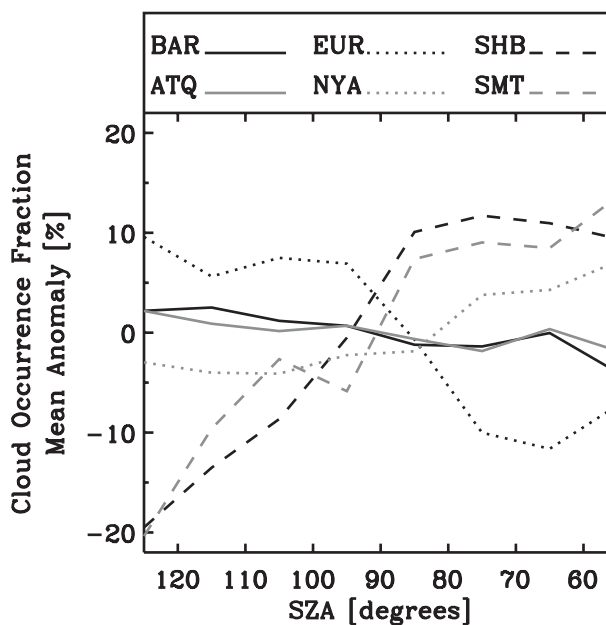


FIG. 9. Mean cloud occurrence fraction anomaly (mean for a given zenith angle minus mean for all zenith angles) as a function of solar zenith angle. Ten-degree-wide bins are used, and each site's latitude determines the relative distribution of data among the different bins (not shown).

One last consideration here is the interannual variability at a given site. The average annual cycles of monthly mean cloud fraction for the multiyear observatories are shown in the top four panels of Fig. 7 along with monthly mean values from individual years. Mean monthly cloud fraction anomalies for these observatories are given in Fig. 7e (see figure caption for definition of these anomalies). At all observatories, the interannual variability of monthly cloud fraction is smallest during the months when the cloud fraction is highest, although the opposite is not always the case. In Eureka, the annual minimum cloud fractions in May and June do correspond with a high interannual variability of about $\pm 13\%$. Ny'Alesund shows the most variability from year to year in terms of both annual and monthly cloud fractions, except for during the summer. The mean year-to-year variability of the annual total cloud fraction for both Alaska sites is less than 3%. Last, despite the relatively high interannual variability in some months, the interannual variability of the annual cloud fraction at Eureka varies by less than $\pm 1\%$, demonstrating a remarkable level of consistency from year to year.

d. Diurnal cycle of cloudiness

The diurnal solar cycle, and its annual variability, in the Arctic are distinct when compared with lower latitudes; the earth's declination leads to long seasons of polar day and night when the sun does not cross the horizon. We

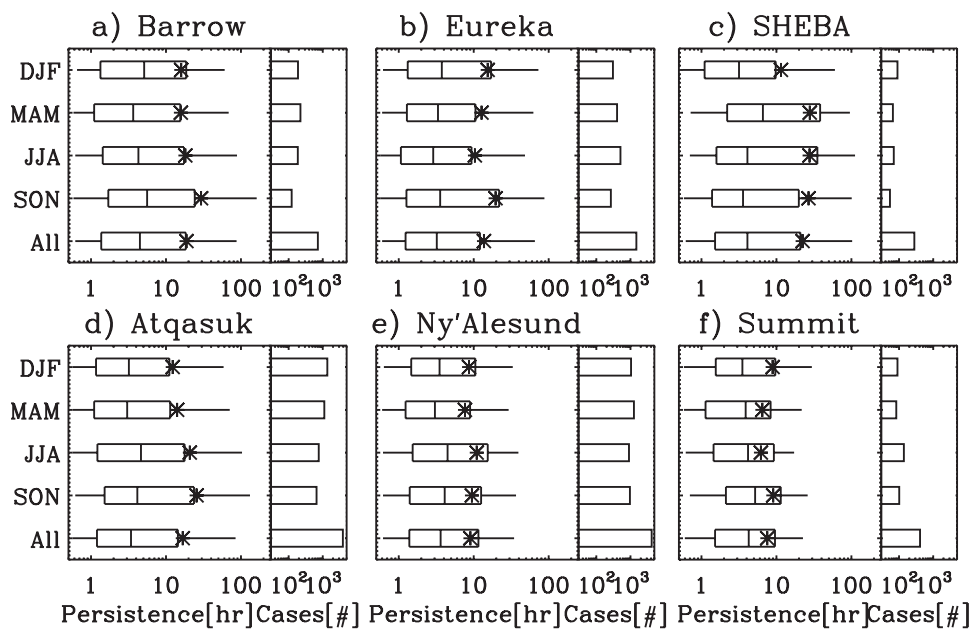


FIG. 10. (a)–(f) Cloud-layer persistence statistics by season at the stations listed. The persistence is defined as the total time that a cloud is continuously observed by the sensors, neglecting interruptions in cloudiness of less than 0.5 h. A minimum persistence of 0.5 h is required. Each panel provides seasonal and full-year statistics (box-and-whiskers diagrams). Box-and-whiskers diagrams include the median (middle bar), 25th and 75th percentiles (ends of box), 5th and 95th percentiles (end of whiskers), and the mean as a symbol. The number of cases contributing to each set of statistics is provided on the right side of each panel.

examine the diurnal cycle of cloud occurrence fraction by distinguishing daily observations into one of three categories: 1) day, where the solar zenith angle (SZA) is less than 90° for the full day; 2) transition, where the SZA is greater than and less than 90° within the day; and 3) night, where the SZA is greater than 90° for the full day. Mean diurnal cloudiness anomalies, defined as the difference between hourly and daily mean cloud fractions, are presented in Fig. 8 and have been adjusted so that the lowest daily SZA for each site is set to approximately 12 h in each plot (see figure caption). Qualitatively, there are weak diurnal cloudiness signatures at some sites during some seasons, which typically manifest as a cloudiness minimum at or closely following solar noon. We speculate that this is related to an increase in solar heating at cloud top at midday resulting in a relative stabilization of the cloud layer leading to somewhat less cloudiness.

For cloud observations made in all seasons (Fig. 8a), the two inland locations at Atqasuk and Summit experience the largest diurnal cycle in cloudiness with amplitudes of 8% and 11%, respectively. SHEBA exhibited a moderate diurnal variation, Ny'Alesund and Barrow have very small diurnal signals, and the Eureka observations depict a small cycle that lags behind those from the other sites by more than 6 h. In each case, the signals are amplified in the day and transition time periods (Figs. 8b and 8c), with

signals as strong as 14%–17% at the inland locations. During the transition period, SHEBA data exhibit a 12% diurnal variability in cloudiness, which is somewhat stronger than the other sites that are influenced by marine environments. The diurnal cycles at coastal sites Barrow, Eureka, and Ny'Alesund are never greater than 8%.

For the supersites, the diurnal cycle is examined at heights below and above 2 km (Figs. 8e–i) to distinguish the impacts of lower-level surface and boundary layer processes from those in the free troposphere, which are more closely associated with synoptic patterns. During SHEBA, the largest diurnal cloudiness signals were observed above 2 km, a pattern that is likely due to the limited sample period at that site. The strongest low-level cycle at SHEBA was in the transition seasons and mirrored the diurnal signature at higher altitudes during those seasons. Barrow generally exhibits more diurnal variability below 2 km than above that height, yet the daily cycles are relatively weak and nonuniform. Eureka tends to have little mean diurnal variability in cloudiness, with only a small signal for low-level clouds during the transition seasons that is delayed from the cycles at the other sites by about 3 h.

Another perspective that complements the diurnal cycle is the association of cloudiness with sun angle. Mean cloud fraction anomalies, or the mean difference between

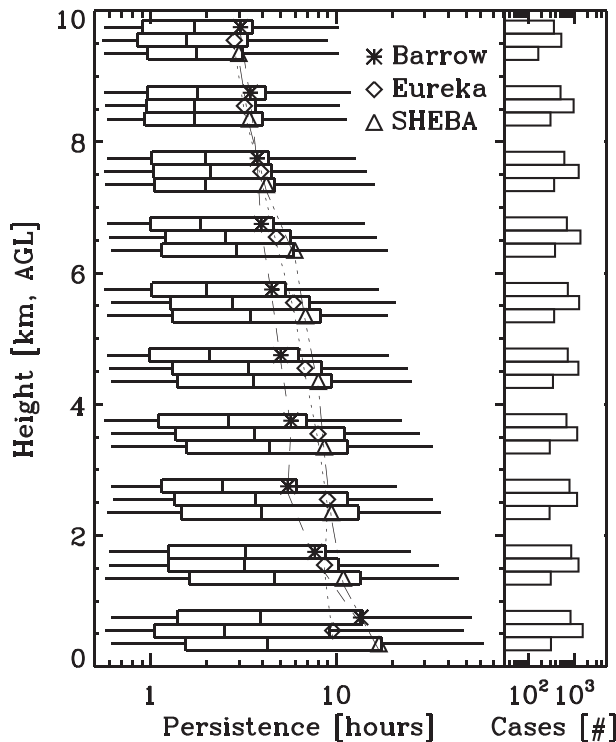


FIG. 11. Cloud-layer persistence with height. Cloud persistence statistics are given in 1-km vertical range bins for Barrow (asterisk), Eureka (diamond), and SHEBA (triangle). Box-and-whiskers diagrams include the median (middle bar), 25th and 75th percentiles (ends of box), 5th and 95th percentiles (end of whiskers), and the mean as a symbol. The number of cases contributing to each set of statistics is provided on the right side.

the mean fraction at a given sun angle and the mean fraction at all angles, are plotted as a function of SZA in Fig. 9, more clearly delineating relationships that can be inferred from Figs. 2 and 3. At the Alaskan sites, total cloud fraction is relatively insensitive to sun angle, on average. This feature occurs because the summer and winter have similar cloud fractions, while the annual maximum and minimum, which occur in the transition seasons at similar sun angles, tend to cancel each other. At the Arctic Ocean site (SHEBA), there was a stark difference in cloudiness demarcated by $SZA = 90^\circ$; clouds were much more frequent with the sun above the horizon. On the contrary, at Eureka less cloudiness occurs when the sun is above the horizon relative to the Polar night. Finally, as the sun reaches higher in the sky, clouds are weakly more prevalent at Ny'Alesund and strongly more prevalent during the year of observations at Summit.

e. Cloud persistence

Cloud-layer persistence has been investigated by examining the continuity of cloud occurrence in the full vertical column. Additionally, at the supersites, persistence has

been examined as a function of height in 0.5-km-thick vertical layers. This analysis does not require that a specific cloud layer be temporally continuous. Instead, some cloud(s) must be continuously present within the height range considered (either the full vertical column or a 0.5-km vertical layer) for at least 30 min, a criterion that removes intermittent cloud layers. Also, for those clouds that meet the first criterion, gaps of less than 30 min are tolerated so that brief breaks in cloudiness, which might be highly localized, are neglected. All cloud persistence information must be considered within the context of the zenith viewing perspective of the ground-based remote sensors. While there is a relationship between persistence at an observatory and spatial cloud coverage, the correlation between these is complicated by spatially stationary systems or topographically influenced cloudiness, which may vary at the different observatories and in time.

Cloud persistence statistics are displayed as a function of season in Fig. 10. Cloudiness tends to be most persistent, on average, in the summer and fall, and least persistent in winter. Exceptions are Eureka and Summit, where minima are observed in summer, while winter clouds are relatively persistent, and during the SHEBA year, where clouds lasted a particularly long time in the spring. These persistence results help to explain many of the broader cloud occurrence fraction results given in Fig. 2, where the highest cloud fractions are typically associated with time periods when clouds are most persistent.

In fall at Barrow, the most persistent cloudiness (top fifth percentile) lasts for more than 160 h, or about 7 days. Over the full year, median cloud persistence ranges from 3.1 to 4.5 h among all sites. At the far western Arctic sites, mean persistence ranges from 17 to 22 h, while at Eureka, Ny'Alesund, and Summit it is 14, 9, and 8 h, respectively. These differences between the mean and median values indicate that in the far western Arctic there are particularly long-lived cloud systems that strongly skew the distribution. The longest-lasting continuous periods of cloudiness at those sites (top fifth percentile) endure for more than 90–100 h, while during the year of observations at Summit, the longest-lasting clouds remained for only about 24 h.

In the vertical, there is a trend toward longer-lasting (or more spatially extensive) clouds closer to the surface (Fig. 11). At the three supersites, the persistence statistics are similar at heights above 7 km. Below that altitude and down to about 2 km, clouds at Eureka and during SHEBA were more persistent than those at Barrow. In the lowest 1 km, Eureka clouds are least persistent relative to Barrow and SHEBA, a trend that may be a result of the more complex topography near Eureka, the colder temperatures, and/or the drier lower troposphere during summer (e.g., Fig. 4). For all three sites together, more than

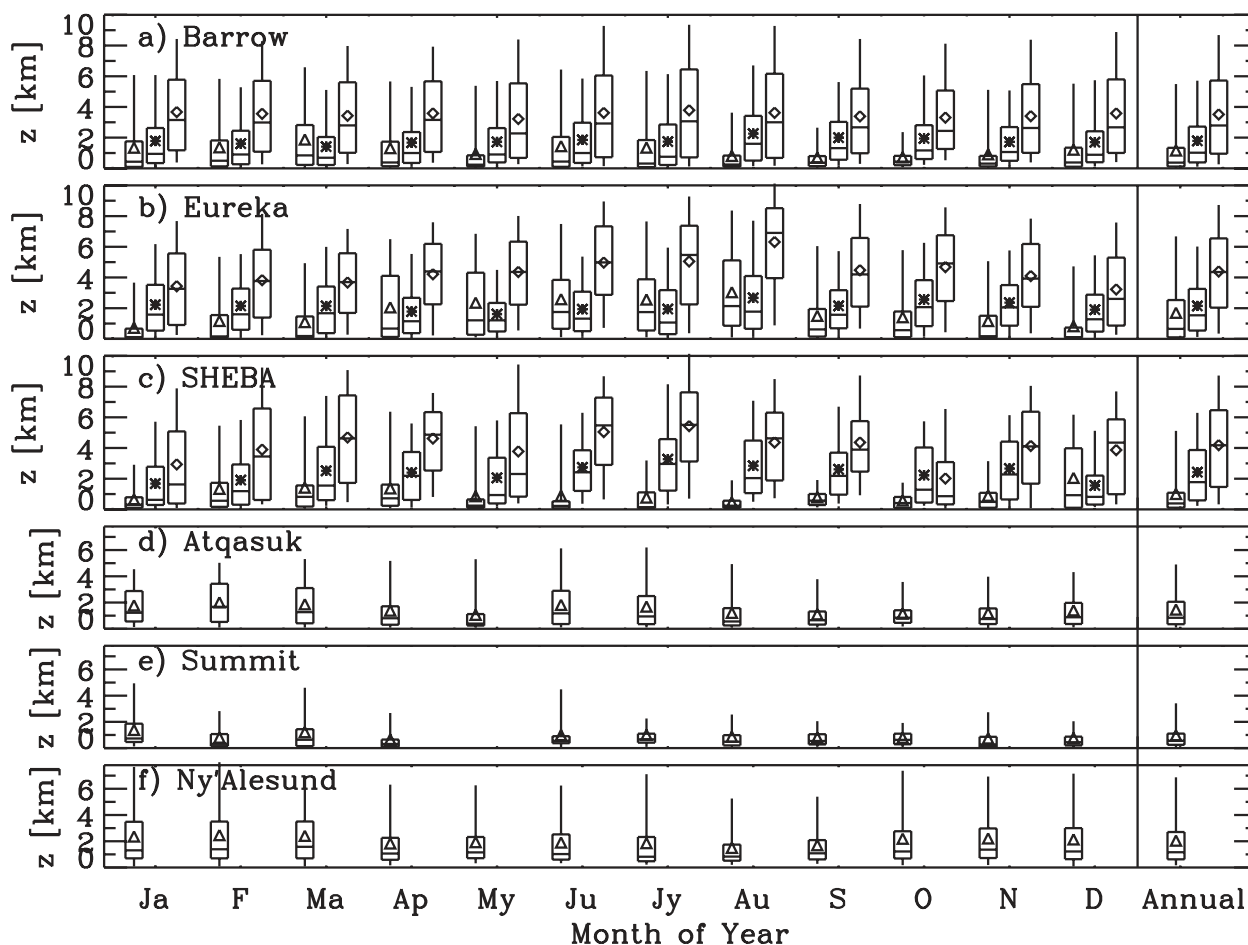


FIG. 12. Cloud boundary and thickness statistics. Each panel shows monthly statistics for low cloud-base height (triangle), total cloud thickness (asterisk), and high cloud-top height (diamond), with the annual means in the right-most column. The lower three panels only contain information on low cloud-base height. Box-and-whiskers diagrams include the median (middle bar), 25th and 75th percentiles (ends of box), 5th and 95th percentiles (end of whiskers), and the mean as a symbol.

5% of the clouds below 1 km persist for longer than 50 h. These vertical profile results help to explain the bulk vertical cloud occurrence fraction results presented in Fig. 3.

f. Cloud boundaries

Statistics characterizing the lowest observed cloud base, highest cloud top, and total cloud thickness are visualized in Fig. 12 using box-and-whiskers plots, which show information on the mean, median, and other percentiles of the data (see figure caption). Cloud-base information is available for each observatory and is most commonly derived from lidar measurements. Cloud-top and -thickness statistics are only available from the supersites.

At the far western Arctic locations (Atqasuk, Barrow, and SHEBA), the lowest cloud-base heights (~ 0.5 km on average) are observed in the summer and fall. At Eureka the highest cloud bases, up to 3 km on average, are

observed in spring and summer, again due to the relative decrease in low-level moisture (Fig. 4e). Comparing the two Alaskan sites, clouds at the inland location of Atqasuk exhibit slightly higher bases than those at the coastal Barrow site, both being near 1 km on average. The annual average cloud-base height at Eureka approaches 2 km. During the year of observations at Summit, monthly mean low cloud-base heights were below roughly 1 km in all months, while in Ny'Alesund, these heights are closer to 2 km. Neither of these sites experiences much seasonal variation in the mean cloud-base height. Note that since the monthly distributions of low cloud-base height are strongly skewed toward higher values, monthly median values are typically lower although the same general trends are apparent. The highest cloud tops are usually observed in the summer at all supersites (as suggested also by Fig. 3). Mean high cloud tops during SHEBA and at Eureka exceeded 4 km, while at Barrow the mean is about 3.5 km. The

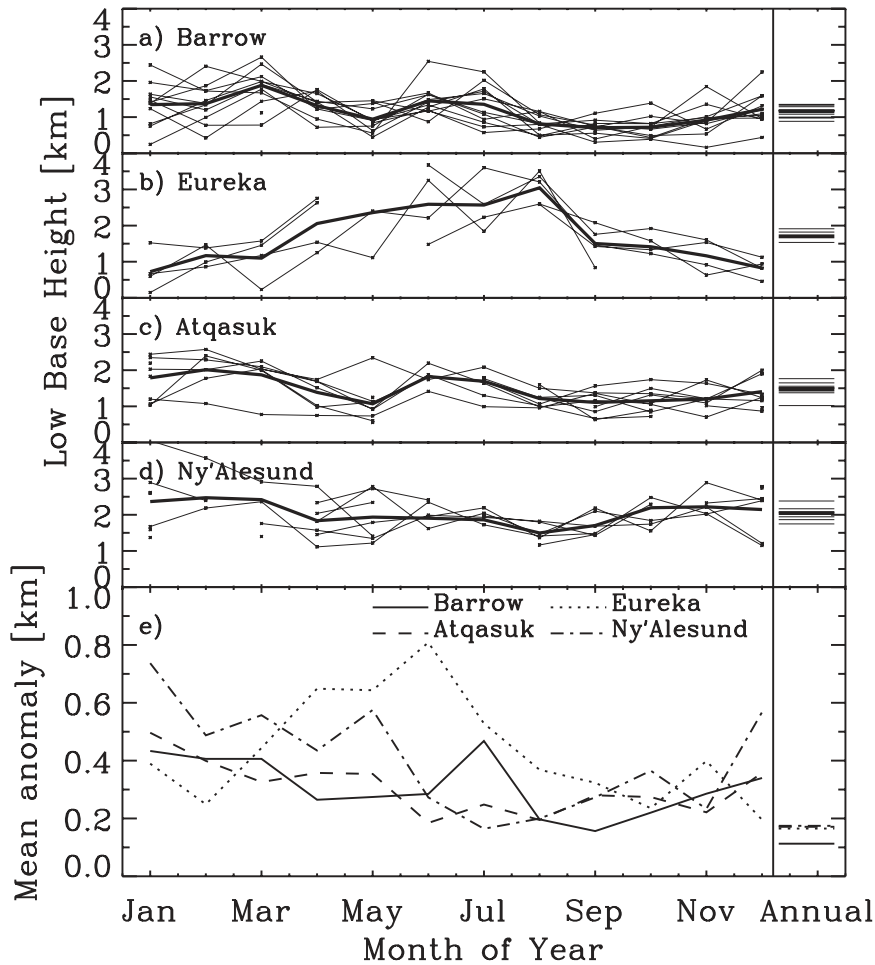


FIG. 13. (a)–(d) Annual cycles of the interannual variability of the mean low cloud-base height for the four stations listed. The site-average annual cycle of the monthly mean low cloud-base height is given (thick line), as well as individual yearly monthly means (dots connected by thin lines). For each time period (month or year) there must be at least 75% data available for a data point to be included. (e) The mean interannual low cloud-base height anomalies for the four stations (thin lines). In all cases, annual means are given in the panels to the right. Anomaly is defined here as the absolute difference between any given monthly mean (e.g., January 2005) relative to the total monthly mean (all Januarys).

total cloud thickness is at or below 2 km at Barrow and Eureka, although Barrow clouds are typically at lower heights in the atmosphere. In comparison, the average cloud thickness from the SHEBA measurements is 2.5 km, which is reflected in the lower mean cloud base and higher mean cloud top when compared with the other supersites.

The interannual variability of cloud boundaries and thicknesses at the multiyear sites is shown in Figs. 13–15. Interannual variability of mean low cloud-base height is relatively consistent among the multiyear observatories (Fig. 13e), although Ny'Alesund shows relatively more variability in the middle of winter and Eureka shows more variability in the spring and summer than the other sites. The mean monthly anomalies (see figure caption for

definition) are around 0.5 km in the winter, and decrease to 0.3 km in the summer when low clouds are frequent at most sites. Annual average low cloud-base heights vary by less than 0.2 km at all sites with the least variability at Barrow. On the contrary, Barrow shows relatively high variability in the highest cloud-top height (Fig. 14), with the most variability in summer. Despite its stronger annual variation in mean high cloud-top height, Eureka shows less variability from year to year in the monthly and annual-mean values. Finally, the interannual variabilities of the monthly mean cloud thickness (Fig. 15) are similar between Barrow and Eureka, while the variability of the annual mean cloud thickness is much smaller at Eureka than Barrow.

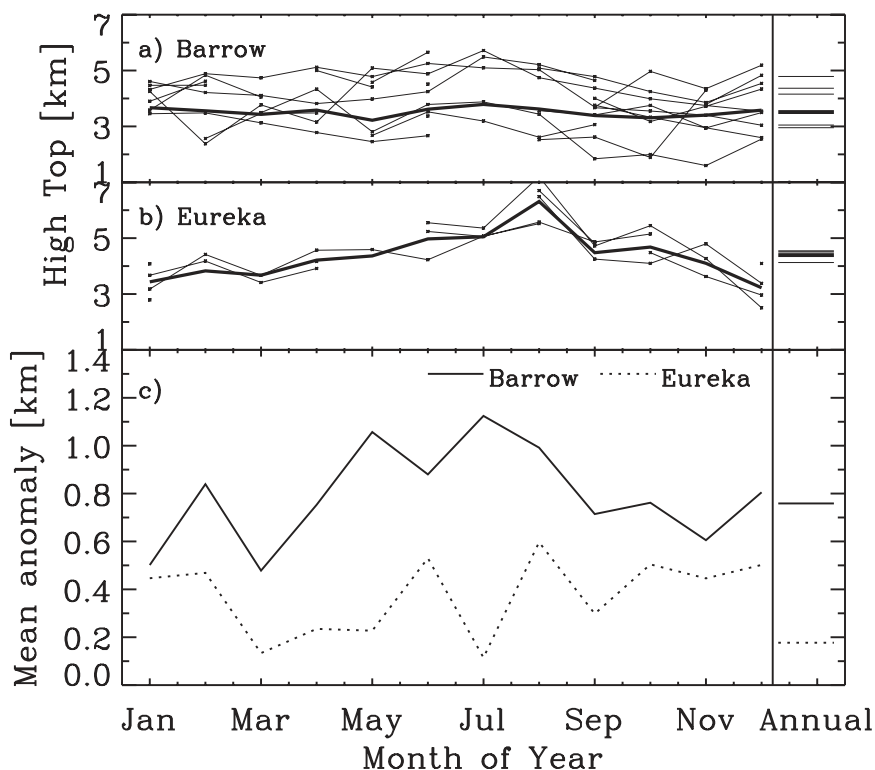


FIG. 14. As in Fig. 13, but for the mean highest cloud top. Multiyear, high cloud-top height data are only available for the Barrow and Eureka sites.

4. Summary

Cloud observations over the past decade from a network of Arctic atmospheric observatories have been investigated in order to characterize Arctic cloud occurrence fraction, macrophysical properties, and persistence. Observatory sites are located in Alaska, Canada, Greenland, Svalbard, and the western Arctic Ocean. Each site facility is equipped with at least one instrument that can identify cloud presence, and three of the sites contain advanced instrument suites that provide information on the vertical distribution of clouds. While the instrument suites and lengths of observations from each site vary significantly, this study has attempted to assemble the existing observations in order to provide a summary of ground-based Arctic cloud observations.

Clouds are observed above these ground-based sites, on average, 58%–83% of the time in any given year, with a typical late summer/fall maximum and a winter minimum. The annual cycle at Eureka is uniquely shifted relative to those at the other stations due to distinct meteorological patterns at that site, which lead to a relative dearth of low-level summer clouds and an abundance of low- and midlevel winter clouds. The annual variability of the monthly cloud fraction is typically 30%–40%, while

observations in Ny'Ålesund show only 20% annual variability. Most sites exhibit interannual variability of less than 13% for monthly cloud fractions and less than 3% for annual cloud fractions. Intersite variability from the all-site mean is typically less than 10%–15% in any given month. These ground-based observations are broadly consistent with previous monthly and annual Arctic surface-observer-based cloud climatologies. An all-site average annual cycle of cloud fraction is similar in magnitude and variability to the Arctic Ocean climatology of Warren et al. (1988). However, the poleward trend toward increased annual cloud variability suggested by Vowinkel and Orvig (1970) is not necessarily supported by these data, and the winter cloud fraction is higher at many sites than suggested by past climatologies.

Cloud occurrence decreases with height from a strong near-surface maximum to a gradual decline with height at middle and upper levels. Of the three supersites, Eureka has the lowest cloud occurrence for low-level clouds (<1 km), while Barrow has a lower fraction of clouds at 2–7 km relative to the observations from Eureka or SHEBA. The median cloud persistence time is 3–5 h at all sites; however, the distributions of persistence at the far western Arctic sites are strongly skewed by the ~5% of clouds that persist longer than 100 h. In contrast, observations at

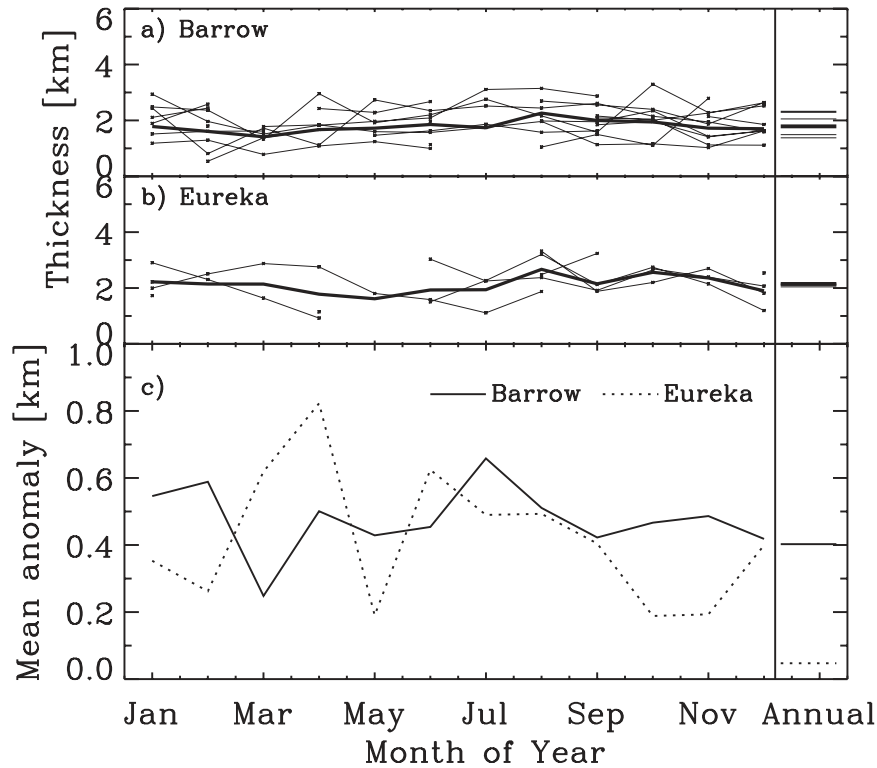


FIG. 15. As in Fig. 13, but for the mean total cloud thickness. Multiyear, total cloud thickness data are only available for the Barrow and Eureka sites.

Summit, Greenland, show few clouds lasting longer than 1 day. As with cloud fraction, persistence decreases with height. Thus, the downward increase in cloud fraction is less due to the frequency of individual clouds than to their perseverance.

On average, only weak diurnal variations in cloudiness are observed, with a minimum occurrence fraction typically near solar noon. The diurnal cycle is strongest (>10% amplitude) at inland sites and during the summer and transition seasons. Total cloud fraction increased as the solar zenith angle decreased in yearlong observations at SHEBA and Summit. At the Alaska sites, little correlation is seen between cloudiness and sun angle. Observations from Eureka, on the other hand, exhibit a decrease in cloud occurrence as the sun reaches higher in the sky.

Relative to other sites, the lowest observed cloud-base height is, on average, lowest at Summit and highest at Ny'Alesund and Eureka. There is a slight suggestion of higher clouds over inland northern Alaska relative to the coast. Interannual variability of the low cloud-base height is usually less than 0.5 km for monthly means and less than 0.2 km for annual means. The total cloud thickness was greater during SHEBA than at Barrow or Eureka.

These results represent a starting point for understanding pan-Arctic cloudiness from ground-based remote sensors.

They provide a foundation for building Arctic cloud climatologies from surface sensors; however, they must be augmented by additional observations over the Arctic Ocean and eastern Arctic in order to broaden our understanding of regional cloud processes. All sites also require longer observational time periods to truly understand the natural variability of cloudiness. However, these results as they currently stand, can serve as a baseline from which to evaluate future changes in cloud occurrence and properties in the western Arctic. In addition, they are suitable for evaluating Arctic model reanalysis datasets and cloud identification algorithms used with satellite observations.

There is still considerable work to be done with regard to a consistent definition of cloudiness that supersedes observing platforms and methods. For example, it is unclear how to specifically combine the high-resolution, diurnal observations at ground-based observatories with the periodic yet spatially extensive cloud observations from a variety of polar-orbiting satellite platforms. An important task ahead will be to bridge these divides in order to optimally combine cloud information from disparate sources and develop a long-term, well-defined, accurate, and spatially extensive estimate of Arctic cloud occurrence and properties.

Acknowledgments. This research was supported by the National Science Foundation Arctic Observing Network Project (ARC 0632187, 0632177, and 0612452) and the Office of Science (BER), U.S. Department of Energy (DE-FG02-05ER63965). Observational data used in this study were provided by the Department of Energy's Atmospheric Radiation Measurement (ARM) Program, the NOAA/Earth System Research Laboratory (ESRL), the Canadian Network for the Detection of Arctic Change (CANDAC), the University of Idaho, the University of Colorado, and the micropulse lidar network (MPLnet). We thank Karen Johnson, Connor Flynn, and David Turner for providing data streams for Barrow.

REFERENCES

- Campbell, J. R., D. L. Hlavka, E. J. Welton, C. J. Flynn, D. D. Turner, J. D. Spinhirne, V. S. Scott, and I. H. Hwang, 2002: Full-time eye-safe cloud and aerosol lidar observations at Atmospheric Radiation Measurement Program sites: Instruments and data processing. *J. Atmos. Oceanic Technol.*, **19**, 431–442.
- , K. Sassen, and E. J. Welton, 2008: Elevated cloud and aerosol layer retrievals from micropulse lidar signal profiles. *J. Atmos. Oceanic Technol.*, **25**, 685–700.
- Clothiaux, E. E., G. G. Mace, T. P. Ackerman, T. J. Kane, J. D. Spinhirne, and V. S. Scott, 1998: An automated algorithm for detection of hydrometeor returns in micropulse lidar data. *J. Atmos. Oceanic Technol.*, **15**, 1035–1042.
- , T. P. Ackerman, G. G. Mace, K. P. Moran, R. T. Marchand, M. Miller, and B. E. Martner, 2000: Objective determination of cloud heights and radar reflectivities using a combination of active remote sensors at the ARM CART sites. *J. Appl. Meteor.*, **39**, 645–665.
- Curry, J. A., 1986: Interactions among turbulence, radiation, and microphysics in Arctic stratus clouds. *J. Atmos. Sci.*, **43**, 90–106.
- , W. B. Rossow, D. Randall, and J. L. Schramm, 1996: Overview of Arctic cloud and radiation characteristics. *J. Climate*, **9**, 1731–1764.
- Dong, X., and G. G. Mace, 2003: Arctic stratus cloud properties and radiative forcing derived from ground-based data collected at Barrow, Alaska. *J. Climate*, **16**, 445–461.
- Eloranta, E. W., 2005: High spectral resolution lidar. *Lidar: Range-Resolved Optical Remote Sensing of the Atmosphere*, K. Weitkamp, Ed., Springer-Verlag 143–163.
- Herman, G. F., and J. A. Curry, 1984: Observational and theoretical studies of solar radiation in Arctic stratus clouds. *J. Climate Appl. Meteor.*, **23**, 5–24.
- Hobbs, J. V., and A. L. Rangno, 1990: Rapid development of high ice particle concentrations in small Polar maritime cumuli-form clouds. *J. Atmos. Sci.*, **47**, 2710–2722.
- , and —, 1998: Microstructures of low- and middle-level clouds over the Beaufort Sea. *Quart. J. Roy. Meteor. Soc.*, **124**, 2035–2071.
- Huschke, R. E., 1969: Arctic cloud statistics from 'air-calibrated' surface weather observations. RAND Corporation Memo. RM-6173-PR, Santa Monica, CA, 79 pp.
- Intrieri, J. M., M. D. Shupe, T. Uttal, and B. J. McCarty, 2002: An annual cycle of Arctic cloud characteristics observed by radar and lidar at SHEBA. *J. Geophys. Res.*, **107**, 8030, doi:10.1029/2000JC000423.
- Jayaweera, K. O. L. F., and T. Ohtake, 1973: Concentration of ice crystals in Arctic stratus clouds. *J. Rech. Atmos.*, **7**, 199–207.
- Kay, J. E., T. L'Ecuyer, A. Gettelman, G. Stephens, and C. O'Dell, 2008: The contribution of cloud and radiation anomalies to the 2007 Arctic sea ice extent minimum. *Geophys. Res. Lett.*, **35**, L08503, doi:10.1029/2008GL033451.
- Knuteson, R. O., and Coauthors, 2004: Atmospheric Emitted Radiance Interferometer. Part I: Instrument design. *J. Atmos. Oceanic Technol.*, **21**, 1763–1776.
- Liljegren, J. C., 1994: Two-channel microwave radiometer for observations of total column precipitable water vapor and cloud liquid water path. Preprints, *Fifth Symp. on Global Change Studies*, Nashville, TN, Amer. Meteor. Soc., 262–269.
- Lubin, D., and A. M. Vogelmann, 2006: A climatologically significant aerosol longwave indirect effect in the Arctic. *Nature*, **439**, 453–456.
- MacDonald, A. E., 2005: A global profiling system for improved weather and climate prediction. *Bull. Amer. Meteor. Soc.*, **86**, 1747–1764.
- McFarquhar, G. M., G. Zhang, M. R. Poellot, G. L. Kok, R. McCoy, T. P. Tooman, and A. J. Heymsfield, 2007: Ice properties of single layer stratocumulus during the Mixed-Phase Arctic Cloud Experiment (M-PACE)—Part 1: Observations. *J. Geophys. Res.*, **112**, D24201, doi:10.1029/2007JD008633.
- Moran, K. P., B. E. Martner, M. J. Post, R. A. Kropff, D. C. Welsh, and K. B. Widener, 1998: An unattended cloud-profiling radar for use in climate research. *Bull. Amer. Meteor. Soc.*, **79**, 443–455.
- Perovich, D. K., J. A. Richter-Menge, K. F. Jones, and B. Light, 2008: Sunlight, water, and ice: Extreme Arctic sea ice melt during the summer of 2007. *Geophys. Res. Lett.*, **35**, L11501, doi:10.1029/2008GL034007.
- Pinto, J. O., 1998: Autumnal mixed-phase cloudy boundary layers in the Arctic. *J. Atmos. Sci.*, **55**, 2016–2038.
- Putnins, P., 1970: The climate of Greenland. *Climates of the Polar Regions*, S. Orvig, Ed., World Survey of Climatology, Vol. 14, Elsevier, 3–128.
- Rossow, W. B., and R. A. Schiffer, 1991: ISCCP cloud data products. *Bull. Amer. Meteor. Soc.*, **72**, 2–20.
- , A. W. Walker, and L. C. Garder, 1993: Comparison of ISCCP and other cloud amounts. *J. Climate*, **6**, 2394–2418.
- Sassen, K., 2005: Dusty ice clouds over Alaska. *Nature*, **434**, 456.
- , and B. S. Cho, 1992: Subvisual-thin cirrus lidar dataset for satellite verification and climatological research. *J. Appl. Meteor.*, **31**, 1275–1285.
- Schweiger, A. J., J. Zhang, R. W. Lindsay, and M. Steele, 2008: Did unusually sunny skies help drive the record sea ice minimum of 2007? *Geophys. Res. Lett.*, **35**, L10503, doi:10.1029/2008GL033463.
- Shupe, M. D., 2011: Clouds at Arctic atmospheric observatories. Part II: Thermodynamic phase characteristics. *J. Appl. Meteor. Climatol.*, **50**, 645–661.
- , T. Uttal, S. Y. Matrosov, and A. S. Frisch, 2001: Cloud water contents and hydrometeor sizes during the FIRE-Arctic Clouds Experiment. *J. Geophys. Res.*, **106**, 15 015–15 028.
- , —, and —, 2005: Arctic cloud microphysics retrievals from surface-based remote sensors at SHEBA. *J. Appl. Meteor.*, **44**, 1544–1562.
- , S. Y. Matrosov, and T. Uttal, 2006: Arctic mixed-phase cloud properties derived from surface-based sensors at SHEBA. *J. Atmos. Sci.*, **63**, 697–711.
- Stephens, G. L., 2005: Cloud feedbacks in the climate system: A critical review. *J. Climate*, **18**, 237–273.

- , and Coauthors, 2002: The CloudSat mission and the A-Train: A new dimension of space-based observations of clouds and precipitation. *Bull. Amer. Meteor. Soc.*, **83**, 1771–1790.
- Turner, D. D., 2005: Arctic mixed-phase cloud properties from AERI-lidar observations: Algorithm and results from SHEBA. *J. Appl. Meteor.*, **44**, 427–444.
- Uttal, T., and Coauthors, 2002: Surface heat budget of the Arctic Ocean. *Bull. Amer. Meteor. Soc.*, **83**, 255–275.
- Vowinkel, E., and S. Orvig, 1970: The climate of the north polar basin. *Climates of the Polar Regions*, S. Orvig, Ed., World Survey of Climatology, Vol. 14, Elsevier, 129–152.
- Wang, X., and J. R. Key, 2003: Recent trends in Arctic surface, cloud, and radiation properties from space. *Science*, **299**, 1725–1728.
- , and —, 2005: Arctic surface, cloud, and radiation properties based on AVHRR Polar Pathfinder dataset. Part I: Spatial and temporal characteristics. *J. Climate*, **18**, 2558–2574.
- Warren, S. G., C. J. Hahn, J. London, R. M. Chervin, and R. L. Jenne, 1988: Global distribution of total cloud cover and cloud type amounts over the ocean. NCAR Tech. Note NCAR/TN-317+STR, 212 pp.
- Welton, E. J., and J. R. Campbell, 2002: Micropulse lidar signal uncertainties. *J. Atmos. Oceanic Technol.*, **19**, 2089–2094.
- Winker, D. M., J. R. Pelon, and M. P. McCormick, 2003: The CALIPSO mission: Spaceborne lidar for observation of aerosols and clouds. *Lidar Remote Sensing for Industry and Environment Monitoring III*, U. N. Singh, T. Itabe, and Z. Liu, Eds., International Society for Optical Engineering (SPIE Proceedings Vol. 4893), 1–11.